Narrowing provenance for ancient Greek silver coins using Ag isotopes and Sb contents of potential ores

Markos Vaxevanopoulos, Gillan Davis, Jean Milot, Janne Blichert-Toft, Chloé Malod-Dognin, Francis Albarède

Narrowing provenance for ancient Greek silver coins using Ag isotopes and Sb contents of potential ores

Markos Vaxevanopoulos[1], Gillan Davis[2], Jean Milot[1], Janne Blichert-Toft[1*], Chloé Malod-Dognin[1], and Francis Albarède[1]

[1] *Ecole Normale Supérieure de Lyon, CNRS, and Université de Lyon, France*

[2] *Australian Catholic University, Sydney, Australia*

**Corresponding author:* Janne Blichert-Toft (jblicher@ens-lyon.fr)

Abstract

Variations of $^{109}Ag/^{107}Ag$ in silver coins and ores are particularly useful in assessing the provenance of silver bullion. Silver isotope variability results from the temperature-dependent thermodynamic fractionation of Ag isotopes among the solutions and minerals participating in ore formation. They differ from lead isotopic variations which result from the decay of uranium and thorium and reflect the geochemical properties and the tectonic age of the possible ore sources. A remarkable property of Ag isotopes is the very narrow range of isotopic variations in silver bullion used for coinage ($\pm 1\times10^{-4}$) with respect to the range of ores ($\pm 1\times10^{-3}$). To test the practical usefulness of the technique, we analyzed the Ag isotopic abundances of 29 ore samples from ancient mining districts in the Aegean with major and minor Ag-bearing mineralizations, and of 34 ancient Greek coins minted from the sixth to late fourth centuries BC. We distinguished two groups among the coins: a dominant population (93% of the samples) with $^{109}Ag/^{107}Ag$ consistent with literature data ($\varepsilon^{109}Ag = -1$ to $+1$) and an isotopically lighter population ($\varepsilon^{109}Ag = -2$ to -1) which we show originated from Ag-bearing mineralizations in Lavrion (Attica). We further found that sulfur (also analyzed in this study) and silver isotope compositions in Aegean ores do not correlate, a finding which we confirmed on a selection of Iberian galena samples. This shows that the genetic ore type (whether hypo, meso, or epithermal) and silver productivity are not related. Finally, we undertook chemical analysis of the Aegean ore samples and confirmed that Ag-rich ores are Sb-rich for both Greece and Iberia.

A remarkable outcome of Ag isotope studies in galena ores from Iberia and Greece is that silver isotope compositions can exclude, with a high degree of reliability, the

majority of mines identified by lead isotope analysis as sources from which coinage silver could plausibly have been extracted and thus significantly narrow down the actual source(s). Silver isotope results on galena ores are thus a useful tool for deciding which Pb isotope data included in ore databases should be included in provenance assessment studies. Contrary to some earlier assessments, subtle silver isotope variations can occasionally help determine ore provenance within a single mining district such as Lavrion.

Keywords: Silver isotopes, antimony, ores, silver coins, Lavrion, Greece

1. Introduction

Silver coins are useful and abundant artefacts for understanding metal circulation in antiquity. Lead isotopic analysis is the predominant method that has been used by archaeometallurgists over the past 50 years to identify the ore sources of ancient silver coins (Gentner et al., 1978; Gale, 1979; Chamberlain and Gale, 1980; Gale et al., 1980; Wagner et al., 1980; Wagner and Weisgerber, 1985; Stos-Gale and Gale, 2009). Technically, the method has problems related to analytical accuracy, ore mineralogy, and the extent to which sampling represents a given source (Vaxevanopoulos et al., 2022). The underlying assumptions are that the lead being measured, which usually represents less than 1% of the mass of the coin (Davis et al., 2020), comes from the same source as the silver and that no foreign lead was added during the cupellation process. This assumption is not unreasonable as most silver-bearing ores, notably argentiferous galena, contain sufficient lead for cupellation. Addition of lead was therefore a necessity only for jarosite ores which do not contain it, notably in a number of ore mineralizations found on the Iberian Peninsula (Milot et al., 2021a). However, there are two concerns which present formidable problems in reliably identifying an ore source. First, geographically distant mining districts may show similar Pb isotopic compositions, and second, a specific mining district may have a range of Pb isotopic compositions (Vaxevanopoulos et al., 2022). This paper's authors have recently revisited the alternative parameterization of Pb isotopes as model ages, U/Pb, and Th/U to good effect as it takes advantage of the accuracy and precision of multiple-collector inductively-coupled plasma mass spectrometry (MC-ICP-MS) Pb isotope analysis and provides a strong geology-oriented diagnostic (Albarède et al., 2012; Milot et al., 2022; Vaxevanopoulos et al., 2022). Nevertheless, overlap between fields remains a major source of ambiguity.

Silver isotopes offer a potential breakthrough since the realization by Fujii and Albarède (2018) and Milot et al. (2022) that, while the range of $^{109}Ag/^{107}Ag$ in silver coins from different periods and places (ancient Greece, ancient Rome, medieval

Europe, colonial Spanish Americas) is extremely narrow (ε^{109}Ag = −1 to +1; Desaulty et al., 2011; Desaulty and Albarède, 2013; Albarède et al., 2016, 2021; *Hacksilber* from the ancient southern Levant: ε^{109}Ag = −2 to +1; Eshel et al., 2022), the range is much broader for silver ores (-8 to +9; Mathur et al., 2018; Arribas et al., 2020; Wang et al., 2022) and for Iberian galena samples (ε^{109}Ag = −8 to +3; Milot et al., 2021a). This stark contrast offers the potential to differentiate Ag-bearing ores that actually may have produced metal used for coinage from other mines which did not contribute to coin production. In addition, the high temperature of metallurgical processes applied to Ag-bearing ores does not cause significant isotopic fractionation (Albarède et al., 2020; Wang et al., 2022). Thus, while Pb isotopes in silver coinage and artefacts allow potential sources to be identified, which are often too many to be of practical use, Ag isotopes allow most of them to be eliminated. It should be noted that the range of values has nothing to do with the resolution. The finding indicates that only certain types of deposit were exploited for Ag production. The possibility that ore sources were mixed for many coins, especially in later periods, cannot always be excluded, but mixing characteristically tends to stretch the range of values along the Pb isotope growth curve (see for example Tell Keisan and Megiddo Hacksilber hoards in Eshel et al., 2021).

We sampled ores from the major ancient mining areas in Greece as well as other districts with minor Ag-bearing mineralizations from which ore is known to have been extracted in antiquity (Vaxevanopoulos et al., 2022) and analyzed Ag and S isotopic abundances together with the concentrations of diagnostically important trace elements, notably antimony (Sb). Here we present Ag isotopic compositions and select trace element concentrations for 29 galena, cerussite, and pyrargyrite-proustite samples from Lavrion, Pangaeon, Siphnos, north-eastern Chalkidiki, Euboea, and six other Ag occurrences in Greece for which ancient mining has not so far been clearly attested (Fig. 1). The companion Pb isotopic compositions are published and discussed in Vaxevanopoulos et al. (2022). We also tested whether sulfur isotopes provide a means for ore source discrimination or offer any other insight into the petrological processes of silver ore formation by measuring δ^{34}S on a subset of the Aegean ores investigated by Vaxevanopoulos et al. (2022) and the Iberian galena samples for which Ag and Pb isotopes are published by Milot et al. (2021a, 2022). Silver isotope abundances are also reported for coins from across the ancient Greek world. The companion Pb isotope data for these coin samples are reported in Blichert-Toft et al. (2022).

2. Materials and Methods

Silver separation for high-precision Ag isotope analysis of ores followed the procedure of Milot et al. (2021b), while for silver coins, Ag separation followed the procedure of Desaulty et al. (2011) as modified by Milot et al. (2021b). Twenty-nine ore samples were collected from 11 different Ag-bearing localities in Greece. After crushing, Ag-rich minerals were separated from gangue minerals (calcite, quartz, fluorite, and feldspars) by handpicking, then powdered by hand in a clean agate mortar. The samples were digested in 10 mL concentrated distilled HNO_3 and dried down at 130°C. Thirty-four silver coins of low numismatic value were purchased from certified numismatic dealers. Given that the outer layer of the coin sample (the patina) is different from the interior due to interaction with groundwater and other contaminants (Gore and Davis, 2016), which affects the Ag isotopic compositions, each coin was drilled on the edge using a 500 µm diameter bit. The surface layer of patina in those cases where patina was observed (Caridi et al., 2013) was discarded, and the rest of the material including only the unoxidized metal was digested in concentrated distilled HNO_3 and evaporated to dryness at 130°C. The samples were then redissolved in 20 mL 3M distilled HNO_3. The concentrations of Ag, Pb, Zn, Cu, As, Bi, Sb, Cd, Sn, Ba, La, and Ce in the 29 ore samples of the main Ag-bearing mineralizations in Greece were measured by quadrupole inductively-coupled plasma mass spectrometry (Q-ICP-MS) at the Ecole Normale Supérieure in Lyon (ENS Lyon).

Silver isotopic compositions, as well as Pb isotopic compositions of two ore samples (THE-01 and THE-7/8) not previously published by Vaxevanopoulos et al. (2022), were analyzed by MC-ICP-MS at ENS Lyon. The Pb isotope compositions of the other ore samples are published in Vaxevanopoulos et al. (2022). Analytical procedures, including precision and accuracy, are described in Milot et al. (2021b).

Sulfur isotope abundances were analyzed commercially at Iso Analytical labs in Crew (England) by Elemental Analysis - Isotope Ratio Mass Spectrometry (EA-IRMS). The technique consists of placing samples and a reference material in tin capsules loaded into an auto-sampler, which in turn is inserted into a furnace at 1080°C and combusted in the presence of oxygen. The combusted gases are swept up in a helium stream over combustion catalysts (tungstic oxide/zirconium oxide) and through a reduction stage of high-purity copper wires to produce SO_2, N_2, CO_2, and water. After the removal of water, the resultant SO_2 enters the ion source of the isotope-ratio mass spectrometer (IRMS) where upon it is ionized and accelerated. Gas species of different masses are separated in a magnetic field, then simultaneously measured on a Faraday cup universal collector array. Both the reference material and the samples are converted to SO_2 and analyzed using this method. The analysis proceeds by batch in each of

which a reference is first analyzed, then followed by a number of samples, then by another reference. The reference material used for sulfur isotope analysis was IA-R061 (barium sulphate, δ^{34}SV-CDT = +20.33 ‰).

3. Results

The Ag isotopic compositions of the 29 ore samples analyzed here from ancient mining areas in Greece are listed in Table 1. The corresponding Pb isotopic compositions, Pb model ages, and μ and κ values published in Vaxevanopoulos et al. (2022) are also included in Table 1 for convenience to the reader, as are the concentrations of Ag, Pb, Cu, As, Bi, Sb, Cd, Sn, Ba, La, and Ce and the sulfur isotopic compositions of a subset of the 29 ore samples. The Ag isotopic compositions are reported on carbonate replacement deposits (Lavrion, Siphnos, Seriphos, Chalkidiki), intrusion-related systems (Euboea, Pangaeon), and epithermal mineralizations (Melos, Antiparos, Lesbos, Kirki, Thera) (Table 1). The ε^{109}Ag scale used as the x-axis in Figs. 2, 3, and 4 represents deviations of the measured sample ^{109}Ag/^{107}Ag ratio from that of the NIST SRM 978a value in parts per 10,000:

$$\left(\frac{^{109}\mathrm{Ag}}{^{107}\mathrm{Ag}}\right)_{sample} = \left(\frac{^{109}\mathrm{Ag}}{^{107}\mathrm{Ag}}\right)_{978\mathrm{A}} \left(1 + \frac{\varepsilon^{109}\mathrm{Ag}}{10{,}000}\right)$$

Confusion may occasionally arise because ore literature often prefers the delta notation δ^{109}Ag (parts per 1000). In this work, the epsilon notation (parts per 10,000) is used specifically to deal with the narrow range of isotopic variations in silver coins. The ε^{109}Ag values of the potential ores vary between -6.10 and +9.20 (Table 1, Figs. 2 and 3). Thirteen samples from the ancient mining district of Lavrion range from -3.67 to +9.2 (Fig. 2). A narrow range of ε^{109}Ag (-0.6 to -1.2) is observed in four samples obtained from the ancient mine in Esperenza-01 (Table 1). A cerussite sample obtained from the ancient Sykia mine in Lavrion, where supergene alteration is abundant, has an ε^{109}Ag of -3.67. Two galena samples from Lavrion with extreme values of +9.2 and +4.6 (Fig. 2) were collected in a modern mine around the Plaka area from Vein 80, which crosscuts the carbonate replacement bodies. No ancient mining activity has been recorded at this locality. The pyrargyrite-proustite sample from the same mineralization has a negative ε^{109}Ag of -1.5 (Table 1), which makes it a potential source of bullion.

The ε^{109}Ag values of samples from the ancient mining areas on the Greek islands of Siphnos, Euboea, Melos, Antiparos, Lesbos, and Thera range from -3.32 to +3.25 (Fig. 2). A positive value of +3.25 was obtained for a cerussite sample from a Siphnos

mineralization in the ancient mine of Aghios Silvestros (Fig. 2), which is related to a highly oxidized mineralization of a carbonate replacement deposit in the central part of the island. For the samples collected in Pangaeon, Chalkidiki, and Kirki (northern Greece), the ε^{109}Ag values range from −6.10 to +1.71 (Fig. 2).

Figure 4a shows sulfur isotopes (δ^{34}S) in Greek (Table 1) and Iberian (Supplementary Material) galena samples as a function of ε^{109}Ag. No significant correlation is observed between the two isotope systems. Figure 4b shows Sb in Greek (Table 1) and Iberian (Milot et al., 2022) galena samples as a function of ε^{109}Ag (Table 1 and Supplementary Material). The high Sb concentrations which are so conspicuous in Iberian galena samples with $-1<\varepsilon^{109}Ag<+1$ (Milot et al., 2022) are also observed in the Greek ore samples of this study for the same ε^{109}Ag interval (Fig. 4b).

Concentrations of a number of trace elements are routinely measured for ore samples together with elements of more manifest interest (Sb, As, Bi, Cu, Zn) and are listed in Table 1 for potential future scrutiny. Most noticeable are the broad concentration ranges of Cd (2.7 to 4752 µg/g) and Sn (up to 3370 µg/g). Bismuth is concentrated in Pangaeon samples P-02 (8312.7 µg/g) and P-04A (7973.8 µg/g) and in Lavrion sample L-25 (1369.7 µg/g) indicative of intrusion-related systems (Lang and Baker, 2001).

The Ag isotopic compositions of the 34 ancient Greek silver coins analyzed here dating from the sixth to the fourth centuries BC are listed in Table 2 and shown in Figs. 2 and 3. Their ε^{109}Ag values range from -1.9 to +0.76. The corresponding Pb isotopic compositions, Pb model ages, and µ and κ values, reported in Blichert-Toft et al. (2022), are included in Table 2 for the convenience of the reader.

The Pb isotopic compositions (Blichert-Toft et al., 2022) of 15 of these coins are consistent with an origin of the silver from ores from Lavrion (Fig. 5). Chalkidiki constitutes another major source of silver with five coins having a high potential for Chalkidiki ore provenance. The Pb isotope data for the other coins overlap with the fields of Thasos, Rhodope, Euboea, Balya, and Kroussia in the Aegean.

4. Discussion

Before suggesting potential provenance and history of the analyzed silver coins, we will first explain the significance of the message conveyed by Ag isotopes. Fujii and Albarède (2018) observed that the ε^{109}Ag of 132 silver coins of different ages from all around the world cluster tightly between −1 and +1 and may be approximated by one, or possibly two, populations. The ε^{109}Ag of a few coins from the present study, in which

we included the five Greek silver coins measured by Desaulty et al. (2011), may be as low as -1.9, which falls slightly outside the range of Fujii and Albarède's single population. This prompted us to evaluate whether these outliers may reveal a mixture of populations, which is better demonstrated by using the empirical cumulative distribution function (Fig. 6) than the histogram of Fig. 3. Histograms (point density functions) are the derivative of the cumulative distribution functions, and as such, they usually look jagged with their ruggedness being particularly sensitive to bin position and width. For this reason, the cumulative distribution function is normally preferred by statistical software to evaluate underlying mixtures of populations. The two-population hypothesis provides an excellent fit with two populations characterized by the following characteristics:

93.5 % for population 1 (av. $\varepsilon^{109}Ag = -0.24 \pm 0.47$) - 41 samples
6.5 % for population 2 (av. $\varepsilon^{109}Ag = -1.81 \pm 0.12$) - 3 samples

Clearly, population 1 tightly overlaps with the range identified by Fujii and Albarède (2018) for worldwide silver coinage. In contrast, population 2 defines a significantly different group with distinctly lower $\varepsilon^{109}Ag$ values. We conclude that the ore sources used for Greek silver coinage span $\varepsilon^{109}Ag>-2$ and $\varepsilon^{109}Ag<1$ but that the values >-1.2 are by far the majority (93%) and are consistent with Fujii and Albarede's (2018) assessment. The dual character of the population of Ag isotope compositions cannot, at this stage, be uniquely explained. Multiple parameters such as a dual sources, temperature, redox conditions, and Rayleigh fractionation (Wang et al., 2022) may, in isolation or in combination, account for the observed dichotomy. Samples are too few and mineralogical and geochemical data on potential ores are too fragmentary to support further speculation at this point.

The present work on Greek mines confirms the suggestion made about Iberian mines (Milot et al., 2021b) that measuring Ag isotopes in galena is important to corroborate the provenance of bullion sources. Lead isotopes show which ore fields are consistent with being bullion sources, and Ag isotopes either confirm or invalidate which of these ore fields are actually suitable bullion sources. We updated the histogram of $\varepsilon^{109}Ag$ values in silver coinage from different origins (Mediterranean, Europe, Americas) and different ages (from the 6th century BC to the 18th century AD) first published by Fujii and Albarede (2018) by including the results from the present work to reach 237 samples (Fig. 7). $\varepsilon^{109}Ag$ values of galena ores from Iberia and the Aegean world are also plotted to emphasize the small fraction of samples which represents suitable bullion sources.

The present work is a caveat that any Pb isotope database used to identify the provenance of coins and other artefacts should ideally be complemented by Ag isotope data. The Ag isotope data on both Iberian and Greek galena samples show that the proportion of galena ores suitable as bullion sources is small (<5%). It is highly predictable that most of the Pb isotope data on ores compiled in OXALID (Stos-Gale and Gale, 2009), IBERLID (Garcia de Madinabeitia et al., 2021), and the databases used by other groups including the authors of the present work contain samples which Ag isotopes would prove could not have been used for bullion production. In addition, keeping in mind that the same silver cannot be hosted in an artefact and in a mine at the same time, implying that the bullion source is by definition missing, and that ancient miners went to great length to extract the last bits of silver ore from each mine, provenance should be assigned by using populations of ores and artefacts rather than by comparing isolated objects and poorly characterized ore samples. This is what statistical methods are striving to remediate to some extent, notably the convex hull approach described by Gentelli et al. (2021) and Blichert-Toft et al. (2022).

The lack of correlation between ε^{109}Ag and δ^{34}S (Fig. 3a) indicates that the petrogenesis of mineralizations is generally of little relevance to the formation of an exploitable mine of silver bullion. As suggested by Fujii and Albarède (2018) and Milot et al. (2021a), the ε^{109}Ag range (−1 to +1 in parts per 10,000) is inherited from the source, most likely from the mantle, with little or no isotope fractionation. The range of Ag isotopic variability in coinage (-1×10^{-4} to $+1\times10^{-4}$) is extremely narrow regardless of its origin (Greece, Iberia, Americas) and calls for a high-temperature origin of the bullion because isotope fractionation among minerals and fluids vanishes at temperatures in excess of ~300°C (Fujii and Albarède 2018). With proper attention paid to the units used by Wang et al. (2022) (parts per 1000 instead of parts per 10,000 as used by Fujii and Albarède [2018]), Rayleigh-type fractional crystallization further enhances isotope fractionation in low- to high-temperature environments and reinforces the necessity of a magmatic or, at the very least, a hypogene origin of the silver used as bullion. In contrast, the ~15 per mil range of δ^{34}S for potential galena sources requiring sulfur isotope fractionation by low- to mid-temperature effects (<300°C) is in stark contrast to the narrow range of Ag isotope variability. The lack of correlation between Ag and S isotope fractionation therefore requires a strong decoupling of the two systems and that Ag went through the final ore-forming process without visible isotope fractionation.

The two cerussite samples analyzed in the present work (with ε^{109}Ag of −3.7 and +3.3) are well outside the silver coinage range. For common silver coins with $-1 < \varepsilon^{109}\text{Ag} < +1$, cerussite deposits cannot have been more than an occasional source of silver for

coinage. This is also the case for the values obtained by Arribas et al. (2020) for two tetrahedrite samples. The low ε^{109}Ag of the cerussite sample from the ancient Sykia mine in Lavrion is not easily explained by the fractionation factors of Fujii and Albarède (2018); oxygen-rich compounds should be isotopically heavy. This is precisely where the Rayleigh distillation effects postulated by Wang et al. (2022) may play a role; the heavy ^{109}Ag isotope is depleted by early precipitation of carbonates or sulfates from low-temperature hydrothermal fluids. This sample can therefore be seen as having been formed from well-ventilated residual solutions circulating in the karst.

Sulfosalts are minerals with the general formula $A_xB_yC_z$, where A typically is monovalent (Ag, Cu), B trivalent (Sb, As, Bi), C mostly sulfur, and x,y,z integer numbers. Minerals such as pyrargyrite (Ag_3SbS_3), proustite (Ag_3AsS_3), tetrahedrite $(Cu,Ag)_6(Sb,As)_4S_{13}$, and miargyrite ($AgSbS_2$) have often been observed in the galena lattice (Voudouris et al., 2008a; 2008b; Bonsal et., 2011). In general, the values of ε^{109}Ag found by Arribas et al. (2020) in pyrargyrite and miargyrite scatter significantly (from −3.3 to +4.9), hence we suggest that sulfosalts within the range of $-2<\varepsilon^{109}Ag<0$ are predominant in Lavrion mineralizations.

The major Greek silver ore is galena, PbS. The Ag and Sb contents of galena are reasonably well correlated (Fig .8). Trace element abundances in ores indicate that the Ag/(Sb+As+Bi) atomic ratio is much lower in galena ores than in most common sulfosalts. With one exception from Iberia, galena samples are characterized by Ag/(Sb+As+Bi)<1, which may be reconciled with the presence of mineralogical end-members or inclusions in galena such as senandorite (a.k.a. andorite VI, $AgPbSb_3S_6$) or freieslebenite ($AgPbSbS_3$). The low Ag/(Sb+As+Bi) ratio of most ores with $-1<\varepsilon^{109}Ag<+1$ therefore suggest that the main ore used for bullion was galena, not sulfosalt. Lavrion with $-2<\varepsilon^{109}Ag<-1$ may have been an exception with a larger contribution of minerals other than galena.

Finally, galena samples with high Sb concentrations have ε^{109}Ag in the same range as the worldwide population of silver coins (−1 to +1) and, therefore, present the strongest potential as candidates for Ag sources for coinage (Milot et al., 2022). This correlation is observed in Greek ores as well and potential sources for silver coinage can be proposed as displayed in Fig. 9. Lavrion samples, such as L-08 and L-09 from Vein 80, a probable mineralization with epithermal affinities (Melfos and Voudouris, 2017), nevertheless are exceptions; despite having high Sb contents, their $\varepsilon^{109}Ag \gg +1$ render them ineligible as a source of bullion.

The authors realize that the first-order rules for using Ag isotopes and Sb concentrations to narrow down acceptable sources of silver as advocated by Milot et

al. (2022) and the present work may have limits. At the present stage, coins with Ag isotope compositions falling significantly outside the range suggested by Fujii and Albarède (2018) have not been recorded. It is possible that small mining operations associated with sulfosalts and unusual minerals may not conform with the broad landscape of Ag isotopes observed for Iberian and Greek mines. At this point, however, available evidence on Ag isotopes in coins and galena samples, and Sb contents in ores, is strong enough to offer useful guidelines for pruning the mines considered potential candidates on the basis of Pb isotopes alone.

5. Conclusions

Silver isotope abundances in sulfide mineralizations show a large spread which contrasts with the narrow range of ε^{109}Ag values characterizing the source of coinage metal. The ε^{109}Ag values of a selection of Greek Ag coinage define two very unequal groups, a dominant population with values indistinguishable from those obtained from around the world for the last 3000 years, and a small population that may originate from Lavrion galena. The narrow range of Ag isotope compositions of silver coinage predicted by Fujii and Albarède (2018) was confirmed by Albarède et al. (2021) for Roman and Greek coinage, by Eshel et al. (2022) for *Hacksilber*, and now again by the present work on Greek coins. This work demonstrates that although lead isotopes are a powerful provenance tool, companion silver isotope data can be used to exclude mine districts that were not actually used as silver ores even though Pb isotopes allow for it. This observation raises the question of the extent to which databases on Pb isotopes in ores should be used. Finally, Ag-rich sulfides, notably galena, are rich in Sb, leaving open the possibility that this element can be used for paleo-environmental applications and to track ancient ores.

Acknowledgements

The senior author acknowledges the European Research Council H2020 Advanced Grant 741454-SILVER-ERC-2016-ADG ‘Silver isotopes and the rise of Money’ for financial support. The Archaeological Ephorates of the East Attica, Cyclades, Euboea, Chalkidiki, Kavala, and Thasos (Greek Ministry of Culture) are thanked for providing permission to conduct ore sampling in the inner parts of the ancient Greek mines investigated in this study. We thank Ryan Mathur and two anonymous reviewers for suggesting multiple clarifications to the text. We further thank Philippe Télouk at ENS Lyon for maintaining the mass spectrometers, and Katrin Westner, Vasilis Melfos, Panagiotis Voudouris, and James Ross for useful suggestions. We appreciate the

assistance in the field of Zacharoula Papadopoulou, Anna Aslanoglou, Kyriaki Fellachidou, and many local people.

References

Albarède, F., Blichert-Toft, J., Gentelli, L., Milot, J., Vaxevanopoulos, M., Klein, S., Westner, K., Birch, T., Davis, G. and de Callataÿ, F., 2020. A miner's perspective on Pb isotope provenances in the Western and Central Mediterranean. Journal of Archaeological Science, 121, 105194. https://doi.org/10.1016/j.jas.2020.105194

Albarède, F., Blichert-Toft, J., De Callataÿ, F., Davis, G., Debernardi, P., Gentelli, L., Gitler, H., Kemmers, F., Klein, S., Malod-Dognin, C., Milot, J., Télouk, P., Vaxevanopoulos and M., Westner, K., 2021. From commodity to money: the rise of silver coinage around the Ancient Mediterranean (sixth–first centuries BCE). Archaeometry 63, pp.142–155. https://doi.org/10.1111/arcm.12615

Albarède, F., Blichert-Toft, J., Rivoal, M. and Telouk, P., 2016. A glimpse into the Roman finances of the Second Punic War through silver isotopes. Geochemical Perspectives Letters, 2(2), pp.127-37.

Albarède, F., Desaulty, A.M. and Blichert-Toft, J., 2012. A geological perspective on the use of Pb isotopes in archaeometry. Archaeometry, 54(5), pp.853-867. https://doi.org/10.1111/j.1475-4754.2011.00653.x

Arribas, A., Mathur, R., Megaw, P. and Arribas, I., 2020. The isotopic composition of silver in ore minerals. Geochemistry, Geophysics, Geosystems, 21(8), p.e2020GC009097. https://doi.org/10.1029/2020GC009097

Blichert-Toft, J., de Callataÿ, F., Télouk, P. and Albarède, F., 2022. Origin and fate of the greatest accumulation of silver in ancient history. Archaeological and Anthropological Sciences, 14(4), pp.1-10. https://doi.org/10.1007/s12520-022-01537-y

Bonsall T.A., Spry P.G., Voudouris P., Tombros S., Seymour K., Melfos V. 2011. The Geochemistry of Carbonate-Replacement Pb-Zn-Ag Mineralization in the Lavrion District, Attica, Greece: Fluid Inclusion, Stable Isotope, and Rare Earth Element Studies. Economic Geology, 106, pp.619-651. https://doi.org/10.2113/econgeo.106.4.619

Caridi, F., Torrisi, L., Cutroneo, M., Barreca, F., Gentile, C., Serafino, T. and Castrizio, D., 2013. XPS and XRF depth patina profiles of ancient silver

coins. Applied Surface Science, 272, pp.82-87. https://doi.org/10.1016/j.apsusc.2012.02.071

Chamberlain, V. and Gale, N.H., 1980. The isotopic composition of lead in Greek coins and in galena from Greece and Turkey. In: Slater, E.A., Tate, J.O. (Eds), Proceedings of the 16th International Symposium on Archaeometry and Archaeological Prospection, Edinburgh 1976. The National Museum of Antiquities of Scotland, pp.139–155.

Davis, G. 2014. Mining money in late Archaic Athens. Historia 63(3), pp.255-277.

Davis, G., Gore, D.B., Sheedy, K.A. and Albarède, F., 2020. Separating silver sources of Archaic Athenian coinage by comprehensive compositional analyses. Journal of Archaeological Science, 114, 105068. https://doi.org/10.1016/j.jas.2019.105068

Desaulty, A.M. and Albarede, F., 2013. Copper, lead, and silver isotopes solve a major economic conundrum of Tudor and early Stuart Europe. Geology, 41(2), pp.135-138. https://doi.org/10.1130/G33555.1

Desaulty, A.M., Telouk, P., Albalat, E. and Albarède, F., 2011. Isotopic Ag–Cu–Pb record of silver circulation through 16th–18th century Spain. Proceedings of the National Academy of Sciences, 108(22), pp.9002-9007. https://doi.org/10.1073/pnas.1018210108

Eshel, T., Gilboa, A., Yahalom-Mack, N., Tirosh, O., and Erel, Y., 2021. Debasement of silver throughout the Late Bronze–Iron Age transition in the Southern Levant: Analytical and cultural implications. Journal of Archaeological Science, 125, 105268.

Eshel, T., Tirosh, O., Yahalom-Mack, N., Gilboa, A. and Erel, Y., 2022. Silver Isotopes in silver suggest Phoenician Innovation in metal production. Applied Sciences, 12(2), 741. https://doi.org/10.3390/app12020741

Fujii, T. and Albarede, F., 2018. ^{109}Ag–^{107}Ag fractionation in fluids with applications to ore deposits, archeometry, and cosmochemistry. Geochimica et Cosmochimica Acta, 234, pp.37-49. https://doi.org/10.1016/j.gca.2018.05.013

Gale, N. H., Gentner, W. and Wagner, G. A., 1980. Mineralogical and geographical silver sources of archaic Greek coinage. Metallurgy in numismatics, 1, pp.3-49.

Gale, N.H., 1979. Lead isotopes and Archaic Greek silver coins. Archaeophysica 10. Rheinisches Landesmuseum Bonn, pp.194–208.

Garcia de Madinabeitia, S. G., Ibarguchi, J. G., and Zalduegui, J. S., 2021. IBERLID: A lead isotope database and tool for metal provenance and ore deposits research. Ore Geology Reviews, 137, 104279.

Gentelli, L., Blichert-Toft, J., Davis, G., Gitler, H. and Albarède, F., 2021. Metal provenance of Iron Age Hacksilber in the southern Levant. Journal of Archaeological Science 134, 105472. https://doi.org/10.1016/j.jas.2021.105472

Gentner, W., Müller, O., Wagner, G.A. and Gale, N.H., 1978. Silver Sources of Archaic Greek Coinage. Naturwissenschaften 65 (6), pp.273–284.

Lang, J. and Baker, T., 2001. Intrusion-related gold systems: the present level of understanding. Mineralium Deposita, 36, pp.477-489.

Mathur, R., Arribas, A., Megaw, P., Wilson, M., Stroup, S., Meyer-Arrivillaga, D. and Arribas, I., 2018. Fractionation of silver isotopes in native silver explained by redox reactions. Geochimica et Cosmochimica Acta, 224, pp.313-326. https://doi.org/10.1016/j.gca.2018.01.011

Melfos, V. and Voudouris, P. 2017. Cenozoic metallogeny of Greece and potential for precious, critical and rare metals exploration. Ore Geology Reviews, 89, pp.1030-1057. https://doi.org/10.1016/j.oregeorev.2017.05.029

Milot, J., Blichert-Toft, J., Sanz, M.A., Fetter, N., Télouk, P. and Albarède, F., 2021a. The significance of galena Pb model ages and the formation of large Pb-Zn sedimentary deposits. Chemical Geology, *583*, 120444. https://doi.org/10.1016/j.chemgeo.2021.120444

Milot, J., Malod-Dognin, C., Blichert-Toft, J., Télouk, P. and Albarède, F., 2021b. Sampling and combined Pb and Ag isotopic analysis of ancient silver coins and ores. Chemical Geology, 564, 120028. https://doi.org/10.1016/j.chemgeo.2020.120028

Milot, J., Blichert-Toft, J., Sanz, M.A., Malod-Dognin, C., Télouk, P and Albarède, F., 2022. Silver isotope and volatile trace element systematics in galena samples from the Iberian Peninsula and the quest for silver sources of Roman coinage, Geology. https://doi.org/10.1130/G49690.1

Picard, O., 2001. La découverte des gisements du Laurion et les débuts de la chouette. Revue Belge Numismatique 147, pp.1-10.

Ross, J., Voudouris, P., Melfos, V., Vaxevanopoulos, M., Soukis, K. and Merigot, K., 2021. The Lavrion silver district: Reassessing its ancient mining history. Geoarchaeology, 36(4), pp.617-642. https://doi.org/10.1002/gea.21852

Stos-Gale, Z.A. and Gale, N.H., 2009. Metal provenancing using isotopes and the Oxford archaeological lead isotope database (OXALID). Archaeological and Anthropological Science, 1 (3), pp.195–213.

Vaxevanopoulos, M., Blichert-Toft, J., Davis, G. and Albarède, F., 2022. New findings of ancient Greek silver sources. Journal of Archaeological Science, 137, 105474. https://doi.org/10.1016/j.jas.2021.105474

Voudouris, P., Melfos, V., Spry, P.G., Bonsall, T., Tarkian, M. and Economou-Eliopoulos, M., 2008a. Mineralogical and fluid inclusion constraints on the evolution of the Plaka intrusion-related ore system, Lavrion, Greece. Mineralogy and Petrology, 93 (1–2), pp.79–110. https://doi.org/10.1007/s00710-007-0218-0

Voudouris, P., Melfos, V., Spry, P.G., Bonsall, T.A., Tarkian, M. and Solomos, Ch., 2008b. Carbonate-replacement Pb–Zn–Ag±Au mineralization in the Kamariza area, Lavrion, Greece: mineralogy and thermochemical conditions of formation. Mineralogy and Petrology, 94 (1–2), pp.85-106. https://doi.org/10.1007/s00710-008-0007-4

Wagner, G. A, Gentner, W., Gropengiesser H. and Gale, N. H. 1980. Early bronze age lead–silver mining and metallurgy in the Aegean: The ancient works on Siphnos. In: Craddock PT (Ed.) Scientific studies in early mining and extractive metallurgy. British Museum Occasional Paper No. 20, pp.63-86.

Wagner, G. A., Weisgerber, G., (Eds). 1988. "Antike Edel- und Buntmetallgewinnung auf Thasos." Der Anschnitt: Beiheft 6, Deutschen Bergbau-Museum Nr. 42. Bochum 1988.

Wang, J.L., Wei, H.Z., Williams-Jones, A.E., Dong, G., Zhu, Y.F., Jiang, S.Y., Ma, J., Hohl, S.V., Liu, X., Li, Y.C. and Lu, J.J., 2022. Silver isotope fractionation in ore-forming hydrothermal systems. Geochimica et Cosmochimica Acta, 332, pp.24-42. https://doi.org/10.1016/j.gca.2022.01.024

FIGURE CAPTIONS

Figure 1. Map of Greek mining districts and ancient city-states discussed in this work.

Figure 2. $\varepsilon^{109}Ag$ of the analyzed ores and coins. The ore data are spatially grouped. Note that the two outliers among Lavrion ores originating from Vein 80 in the Plaka area where no ancient activity is attested have highly positive $\varepsilon^{109}Ag$.

Figure 3. Histogram of $\varepsilon^{109}Ag$ of the 34 Greek silver coins of this study and 5 coins from Desaulty et al. (2011). The red lines are the two fitted normal distributions discussed below (see scale on the right-hand side).

Figure 4. (Left-hand-side panel) $\delta^{34}S$ of Greek and Iberian galena samples as a function of $\varepsilon^{109}Ag$. The lack of correlation between $\delta^{34}S$ and $\varepsilon^{109}Ag$ indicates a lack of fractionation between coexisting species during low-to middle-temperature petrological process. (Right-hand-side panel) Sb concentrations of Greek and Iberian galena samples as a function of $\varepsilon^{109}Ag$. The peak of Sb concentrations is observed at around $\varepsilon^{109}Ag\sim0$ in Greek ore samples. A similar Sb peak, also at around $\varepsilon^{109}Ag\sim0$, was previously identified by Milot et al. (2022) in Iberian galena samples. The high Sb contents of the Lavrion samples with the highest $\varepsilon^{109}Ag$ correspond to Vein 80 (Lavrion), which was not exploited in ancient times.

Figure 5. Lead isotope compositions and Pb model ages, μ, and κ in Greek ore samples (Vaxevanopoulos et al., 2022) and Greek silver coins (red upward-pointing triangles; Blichert-Toft et al., 2022).

Figure 6. Fit of the $\varepsilon^{109}Ag$ distribution in silver coins by a cumulative density function formed by the mixing of two distinct populations 1 and 2. The worldwide range ($-1<\varepsilon^{109}Ag<+1$) is from Fujii and Albarède (2018) and this work.

Figure 7. Histogram of $\varepsilon^{109}Ag$ values in silver coinage (this work, Desaulty et al., 2011, 2013; Albarede et al., 2016, 2021). *Hacksilber* analysis by Eshel et al. (2022) are consistent with this range. The $\varepsilon^{109}Ag$ values of galena ores are from this work and Milot et al. (2022).

Figure 8. Correlation between Pb-normalized Ag and Sb+As+Bi concentrations (atomic ratios). The dotted symbols have $\varepsilon^{109}Ag$ values in the interval -1 to +1.1, which qualifiy these samples as potential bullion sources. The Ag/(Sb+As+Bi) is in many cases lower than the ratio in sulfosalts (3 to 1) which, in contrast, does not support these minerals as bullion sources.

Figure 9. Geographic distribution of mining districts that can be accepted as potential sources for the silver of the main population 1 (in red). Galena samples are depicted with full circles and other ores with crosses. Lavrion, Melos, Seriphos, Santorini, Euboea, NE Chalkidiki, and Kirki are among the most likely localities. The color bar on the right-hand side shows the ε^{109}Ag color scale used for the symbols. The red color highlights the range of values (–1 to +1) found in silver coinage.

TABLE CAPTIONS

Table 1. High-precision Ag isotopic compositions of 29 samples from 11 different Ag-bearing mineralizations in Greece for which, in most cases, there is evidence of ancient mining activity. Lead isotopic concentrations, T_{mod}, μ, and κ values are also included, calculated according to Albarède and Juteau (1984). Lead isotopic values are published in Vaxevanopoulos et al. (2022) except for samples THE-01 and THE-7/8. Coordinates for each sample, trace element concentrations, and S isotopic compositions are also included.

Table 2. High-precision Ag and Pb isotopic compositions of 34 drilled coins from Greek city-states in Minor Asia, the Greek mainland, the Black Sea, Sicily, and southern Italy. The Pb isotope data, T_{mod}, μ, and κ values are from Blichert-Toft et al. (2022).

Table 1

Sample	Region	District / Mine	Ore type	Main Mineral[1]	$^{206}Pb/^{204}Pb$[2]	$^{207}Pb/^{204}Pb$[2]
L-06	Lavrion	Jean Vaptiste	Carbonate replacement	Gn	18.8599	15.6837
L-07	Lavrion	Esperanza	Carbonate replacement	Gn	18.8607	15.6872
L-08	Lavrion	Plaka-80	Epithermal	Gn	18.8906	15.7093
L-09	Lavrion	Plaka-80	Epithermal	Gn	18.8845	15.7034
L-10	Lavrion	Dimoliaki	Carbonate replacement	Gn	18.8741	15.6921
L-11	Lavrion	Plaka-145	Carbonate replacement	Gn	18.8762	15.6918
L-12	Lavrion	Esperanza	Carbonate replacement	Gn	18.8649	15.6901
L-13	Lavrion	Esperanza	Carbonate replacement	Gn	18.8670	15.6905
L-14	Lavrion	Esperanza	Carbonate replacement	Sp	18.8594	15.6845
L-17	Lavrion	Poundazeza	Carbonate replacement	Gn	18.8764	15.6941
L-25	Lavrion	Plaka-80	Carbonate replacement	Pyrg-Pr	n.a.	n.a.
L-40	Lavrion	Sykia	Carbonate replacement	Cer	18.8602	15.6995
L-42	Lavrion	Christiana	Carbonate replacement	Gn	18.8642	15.6840
E-05	S Euboea	Moskies	Intrusion Related	Gn	18.6893	15.7011
E-06	S Euboea	Moskies	Intrusion Related	Gn	18.6869	15.6994
SI-10	Siphnos	Agios Silvestros	Carbonate replacement	Wlm-Cer	18.7361	15.7040
SE-03	Seriphos	Moutoula-08	Carbonate replacement	Gn	18.9024	15.7030
M-01A	Melos	Agios Nikolaos	Epithermal	Gn-Sp	18.8601	15.6892
M-01B	Melos	Agios Nikolaos	Epithermal	Gn-Sp	18.8619	15.6896
AN-02	Antiparos	Monastiria	Epithermal	Gn	18.8392	15.7258
LES-01	Lesbos	Argenos	Epithermal	Gn	18.6284	15.6922
OL-01A	NE Chalkidiki	Olympiada	Carbonate replacement	Gn	18.7805	15.6760
PA-02	Pangaeon	Asimotrypes	Intrusion Related	Gn	18.7013	15.6805
PA-04A	Pangaeon	Asimotrypes	Intrusion Related	Gn-Sp	18.7012	15.6835
PA-06	Pangaeon	Avgo peak	Intrusion Related	Gn	18.6948	15.6820
KIR-02	Kirki	Saint-Philippos	Epithermal	Sp-Gn	18.7155	15.6696
KIR-03	Kirki	Saint-Philippos	Epithermal	Sp-Gn	18.7170	15.6691
THE-01	Thera	Athinios	Epithermal	Gn	18.9662	15.6974
THE-7/8	Thera	Athinios shore	Epithermal	Gn	18.9653	15.6983

[1] Abbreviations: Cer=Cerussite, Gn=Galena, Pr=Proustite, Pyrg=Pyrargyrite, Sp=Sphalerite, Wlm=Willemite

[2] Lead isotopic data and Ag-Pb concentrations from Vaxevanopoulos et al. (2022)

n.a.: not analyzed

$^{208}Pb/^{204}Pb^{2}$	longitude	latitude	T_{mod} (Ma)	μ	k	$\varepsilon^{109}Ag^{*}$	2s	$\delta^{34}S^{*}$	Ag μg/g	Pb %
38.825	37° 43' 42.7689" N	24° 00' 38.2815" E	26	9.85	3.85	-1.15	0.33	-3.84	1673	70.7
38.824	37° 43' 34.3682" N	24° 01' 58.0272" E	32	9.86	3.85	-0.79	0.15	n.a.	1264	55.1
38.938	37° 45' 36.1342" N	24° 01' 59.6156" E	54	9.94	3.89	9.20	0.16	-0.63	1656	52.0
38.923	37° 45' 35.8797" N	24° 01' 57.0971" E	46	9.92	3.89	4.62	0.13	-0.29	3029	65.7
38.878	37° 45' 11.1933" N	24° 00' 06.0347" E	32	9.88	3.87	-0.92	0.21	-2.22	1182	32.5
38.893	37° 45' 35.5808" N	24° 02' 01.0620" E	30	9.87	3.87	-0.14	0.21	-0.42	5872	65.7
38.838	37° 43' 34.1947" N	24° 02' 01.7645" E	35	9.87	3.85	-0.58	0.14	1.30	1959	79.3
38.837	37° 43' 34.1947" N	24° 02' 01.7645" E	34	9.87	3.85	-0.73	0.42	n.a.	2005	69.8
38.857	37° 43' 34.4729" N	24° 02' 01.3349" E	28	9.85	3.86	-1.16	0.18	n.a.	330	1.0
38.913	37° 40' 51.8589" N	24° 04' 03.8284" E	29	9.86	3.86	-0.77	0.28	-0.13	4220	55.6
n.a.	37° 45' 36.1342" N	24° 01' 59.6156" E	-	-	-	-1.54	0.17	0.44	7850	1.9
38.889	37° 41' 58.1481" N	24° 00' 38.6262" E	57	9.91	3.88	-3.67	0.72	-3.29	1037	42.9
38.830	37° 44' 02.4144" N	24° 01' 10.9848" E	23	9.85	3.85	-1.74	0.15	-3.28	3951	70.4
38.916	38° 06' 15.6060" N	24° 30' 38.9232" E	186	9.95	4.01	1.71	0.19	6.19	291	89.2
38.913	38° 06' 17.2800" N	24° 30' 39.5208" E	184	9.94	4.01	0.33	0.37	6.67	192	80.6
38.951	37° 00' 22.4271" N	24° 42' 23.6622" E	157	9.95	4.00	3.25	0.27	9.61	4983	7.1
39.014	37° 11' 12.1704" N	24° 30' 06.5340" E	32	9.91	3.92	-0.99	0.37	2.47	470	85.2
39.007	36° 42' 23.5944" N	24° 20' 47.9112" E	36	9.87	3.94	0.83	0.38	1.73	2389	66.4
39.008	36° 42' 23.5944" N	24° 20' 47.9112" E	36	9.87	3.94	-0.32	0.81	n.a.	2473	28.2
39.170	37° 00' 10.7244" N	25° 02' 00.1500" E	123	10.01	4.05	-3.32	0.21	13.89	340	55.8
39.010	39° 22' 38.7120" N	26° 15' 04.8636" E	213	9.92	4.08	-2.09	0.38	-3.46	637	43.1
38.877	40° 35' 11.0020" N	23° 45' 00.6924" E	70	9.83	3.92	-1.14	0.31	-0.68	1536	55.0
38.819	40° 54' 56.0765" N	24° 06' 37.9461" E	137	9.86	3.94	-4.38	0.23	0.99	9697	22.4
38.823	40° 54' 56.0765" N	24° 06' 37.9461" E	143	9.88	3.95	-6.10	0.48	0.72	5439	11.4
38.826	40° 54' 30.6504" N	24° 06' 26.9100" E	145	9.87	3.95	-1.90	0.12	0.30	145	5.7
38.881	41° 01' 16.1292" N	25° 49' 03.5579" E	105	9.82	3.96	1.71	0.18	6.19	949	2.0
38.878	41° 01' 16.1292" N	25° 49' 03.5579" E	103	9.82	3.96	0.04	0.41	1.62	1045	0.3
39.041	36° 23' 18.6288" N	25° 25' 58.0944" E	-26	9.88	3.88	-0.29	0.16	-2.22	2569	54.7
39.013	36° 23' 28.8096" N	25° 25' 57.9180" E	-24	9.88	3.87	1.70	0.07	0.98	2173	86.6

Zn %	Cu µg/g	As µg/g	Bi µg/g	Sb µg/g	Cd µg/g	Sn µg/g	Ba µg/g	La µg/g	Ce µg/g
0.0	864	23342	0.0	2219	9.6	0.0	13.6	7.3	5.1
0.4	230	6	n.a.	2485	14.7	0.5	13.7	0.5	n.a.
1.7	1487	1346	n.a.	7067	231.9	16.6	0.0	3.1	n.a.
0.1	1394	16413	n.a.	11414	16.0	9.3	0.0	0.2	n.a.
13.2	255	316	n.a.	2165	1275	142	41	6.8	n.a.
0.4	662	554	n.a.	15091	45.1	11.3	6.1	0.7	n.a.
0.6	294	5	2.8	2141	28.5	0.0	29	15.0	89
0.7	300	0	3.4	2021	28.3	0.2	14.1	2.7	5.2
56.5	10895	16	1.9	1055	4752	0.0	0.0	5.1	5.2
0.4	514	10166	6.2	10227	57.5	11.6	5.2	3.9	6.5
3.1	5484	22328	1369.7	34099	78.7	3371	916	72.2	25
0.2	1886	0	0.0	1046	183	0.0	0.0	53.5	49
0.2	1692	21408	0.0	2325	2.7	0.0	0.0	8.8	7.3
0.0	190	0	0.0	0	6.0	0.0	0.0	0.0	0.0
0.0	192	0	0.0	0	8.1	0.0	12.4	0.0	0.0
10.1	168	5766	0.0	2446	369.3	0.0	3.9	1.1	1.7
0.8	240	3548	0.0	916	58.4	0.0	17.3	1.4	1.6
27.0	27295	2718	0.0	18393	1811.7	0.0	236	0.2	1.0
17.0	18390	2562	0.0	11250	1423.2	0.0	454	23	11.6
0.4	167	799	0.0	0	6.7	0.0	28	13.9	15.5
0.0	17172	0	520.8	0	4.3	0.0	354	0.4	0.5
11.3	19498	2067	0.0	1776	835.7	71.0	0.0	0.0	0.3
1.5	106588	111016	8312.7	351	159.5	25.5	15.3	6.7	7.9
8.6	98577	17752	7973.8	0	757.5	13.9	0.0	0.7	0.7
0.4	3849	6582	213.9	2957	40.2	0.0	4.5	3.7	1.2
3.7	36875	11699	506.2	1671	379.2	288	235180	12.4	11.8
3.3	33187	26667	19.4	536	14.5	726	3064	4.5	2.7
0.7	498	636	2.0	350	10.6	2874	118.1	15.0	17.5
0.0	217	197	0.0	9.3	5.1	44	0.0	0.6	0.8

Table 2

Sample	Mint	Area	Denomination	Date BC	Weight (g)	$^{206}Pb/^{204}Pb$[1]	$^{207}Pb/^{204}Pb$[1]
P275	Miletus	Ionia	Obol	600-500	1.16	18.8037	15.6596
P276	Abdera	Thrace	Obol	475-450	0.59	18.8259	15.6736
P281	Miletus	Ionia	Obol	500	1.08	18.8544	15.6853
P289	Byzantium	Thrace	Siglos	387-340	2.41	18.7904	15.6799
P290	Chersonesus	Thrace	Hemidrachm	386-338	1.86	18.7347	15.6541
P291	Magnesia	Ionia	Hemidrachm	350-325	1.45	18.7738	15.6586
P293	Cyzicus	Mysia	Hemiobol	450-400	0.36	18.7477	15.6733
P294	Abydos	Troas	Hemidrachm	350-325	2.52	18.8183	15.6839
P297	Cyzicus	Mysia	Drachm	390-341	2.14	18.8324	15.6840
P300	Tenedos	Troad	Obol	450-387	0.59	18.8350	15.6815
P302	Miletus	Ionia	1/48 stater	525-494	0.20	18.8457	15.6782
P303	Unknown	Pandosia[3]	Obol	510	0.57	18.7882	15.6498
P306	Unknown	Lycia	Obol	440-410	0.64	18.7964	15.6741
P307	Chersonesus	Thrace	Hemidrachm	400-338	2.32	18.8233	15.6717
P308	Chersonesus	Thrace	Hemidrachm	400-338	2.31	18.8212	15.6640
P310	Thasos	Thrace	Hemiobol	411-404	0.39	18.6088	15.6452
P311	Miletus	Ionia	Half stater	650-500	1.08	18.7974	15.6526
P313	Argos	Peloponnese[4]	Triobol	480-430	2.86	18.8439	15.6778
P314	Chersonesus	Thrace	Hemidrachm	400-338	2.20	18.8385	15.6792
P316	Thasos	Thrace	Trihemiobol	404-355	0.78	18.7874	15.6696
P317	Thasos	Thrace	Diobol	525-480	0.88	18.8478	15.6693
P318	Chersonesus	Thrace	Hemidrachm	400-338	2.13	18.7883	15.6586
P319		Caria	Tetartemorion	392-377	0.18	18.8186	15.6674
P320	Chersonesus	Thrace	Hemidrachm	400-338	2.26	18.8163	15.6628
P321	Cyzicus	Mysia	Obol	525-475	0.87	18.7939	15.6656
P322	Phocaea	Ionia	Hemihekte	550-500	1.16	18.6235	15.6554
P323	Panticapaion	Tauric Chersonese	Hemiobol	480-470	0.61	18.8388	15.6769
P325	Corinth	Peloponnese[5]	Diobol	500-450	0.62	18.8091	15.6661
P326	Cyzicus	Mysia	Obol	450-400	0.79	18.7782	15.6725
P327	Aegina	Aegina	Obol	525-500	1.03	18.6983	15.6575
P328	Colophon	Ionia	Drachm	322-319	3.85	18.8257	15.6946
P329	Cyzicus	Mysia	Diobol	480-400	1.15	18.7623	15.6550
P330	Cyzicus	Mysia	Obol	480	0.85	18.8502	15.6828
P331	Corinth	Peloponnese[5]	Stater	340	8.13	18.8440	15.6783

[1] Lead isotope data from Blichert-Toft et al. (2022)

[2] Albarede and Juteau (1984)

[3] Bruttium

$^{208}Pb/^{204}Pb$[1]	T_{mod} (Ma)[2]	μ^2	κ^2	$\varepsilon^{109}Ag$	2s
38.8773	19	9.76	3.89	0.17	0.09
38.8303	31	9.81	3.85	-1.63	0.09
38.8366	33	9.85	3.84	0.65	0.09
38.8553	70	9.84	3.89	-0.02	0.15
38.7725	60	9.76	3.88	-0.58	0.06
38.7645	40	9.77	3.85	-0.05	0.05
38.8196	89	9.83	3.90	0.08	0.08
38.8674	57	9.85	3.88	0.03	0.07
38.8554	47	9.85	3.87	-0.58	0.15
38.8326	40	9.84	3.85	-0.43	0.07
38.8298	25	9.83	3.84	0.35	0.09
38.8420	11	9.73	3.87	0.16	0.06
38.7932	54	9.82	3.85	-0.57	0.16
38.8402	29	9.81	3.86	-0.45	0.08
38.7957	15	9.78	3.84	-0.48	0.13
38.7260	137	9.75	3.93	-0.75	0.17
38.8625	10	9.74	3.88	-0.79	0.08
38.8380	26	9.83	3.85	-0.50	0.05
38.8399	33	9.83	3.85	-1.30	0.09
38.8737	52	9.81	3.90	-0.25	0.05
38.9599	6	9.79	3.90	0.58	0.05
38.8550	29	9.76	3.88	-1.04	0.13
38.8305	24	9.79	3.86	-1.16	0.07
38.7980	16	9.77	3.84	-0.64	0.08
38.8897	39	9.79	3.90	-0.69	0.12
38.6796	146	9.78	3.90	-0.66	0.12
38.8373	28	9.82	3.85	-0.15	0.06
38.7954	28	9.79	3.84	-0.36	0.13
38.8108	64	9.82	3.87	-0.27	0.08
38.8046	94	9.78	3.92	0.76	0.08
38.9493	73	9.89	3.92	0.23	0.09
38.8133	41	9.75	3.88	-1.92	0.17
38.8567	31	9.84	3.85	-0.29	0.05
38.8204	27	9.83	3.84	-1.85	0.07

[4] Argolis [5] Corinthia

Fig. 01

Click here to access/download;Figure;FIG. 01.jpg

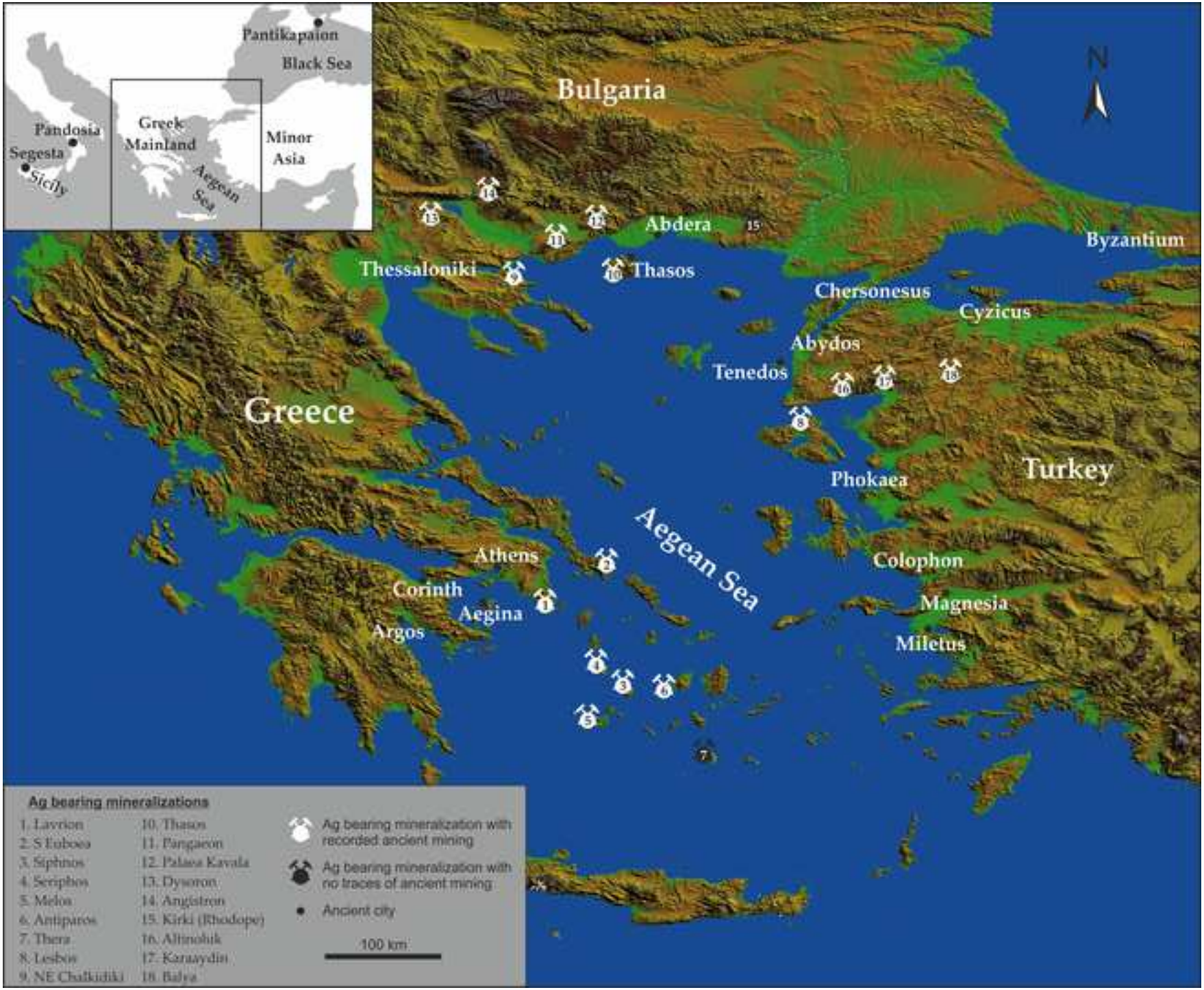

Fig. 02

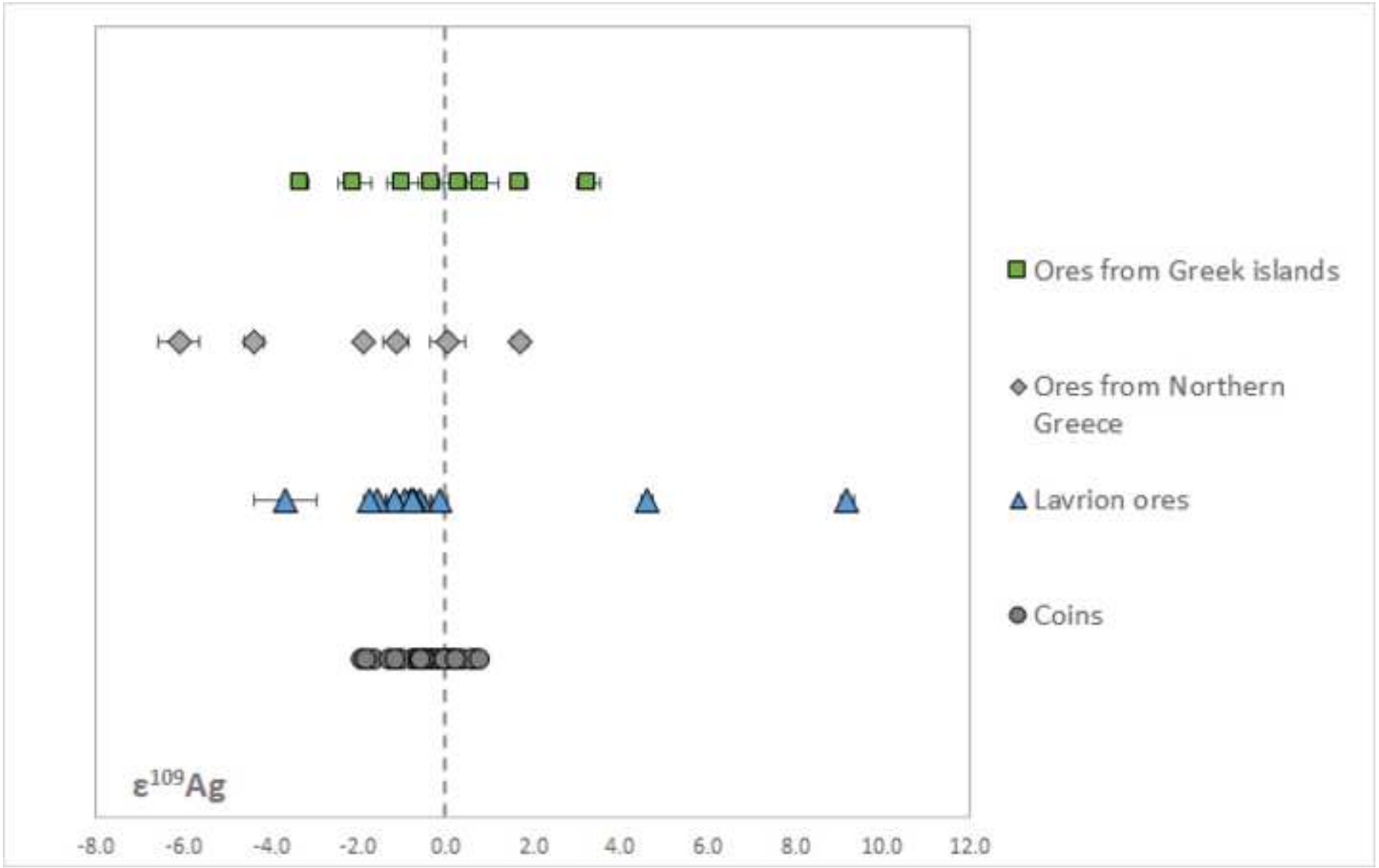

Fig. 03

Click here to access/download;Figure;Fig. 03.jpg

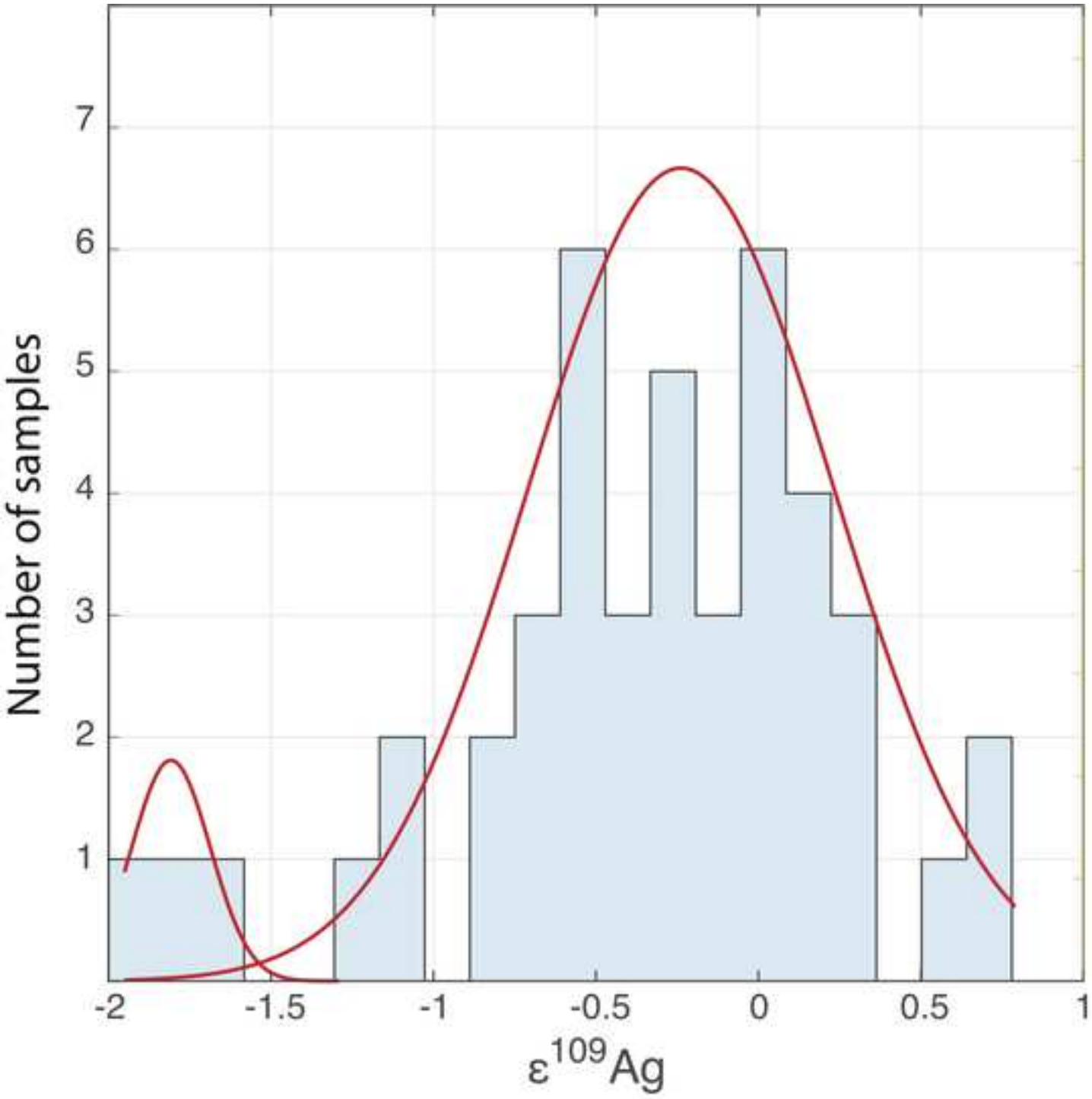

Fig. 04

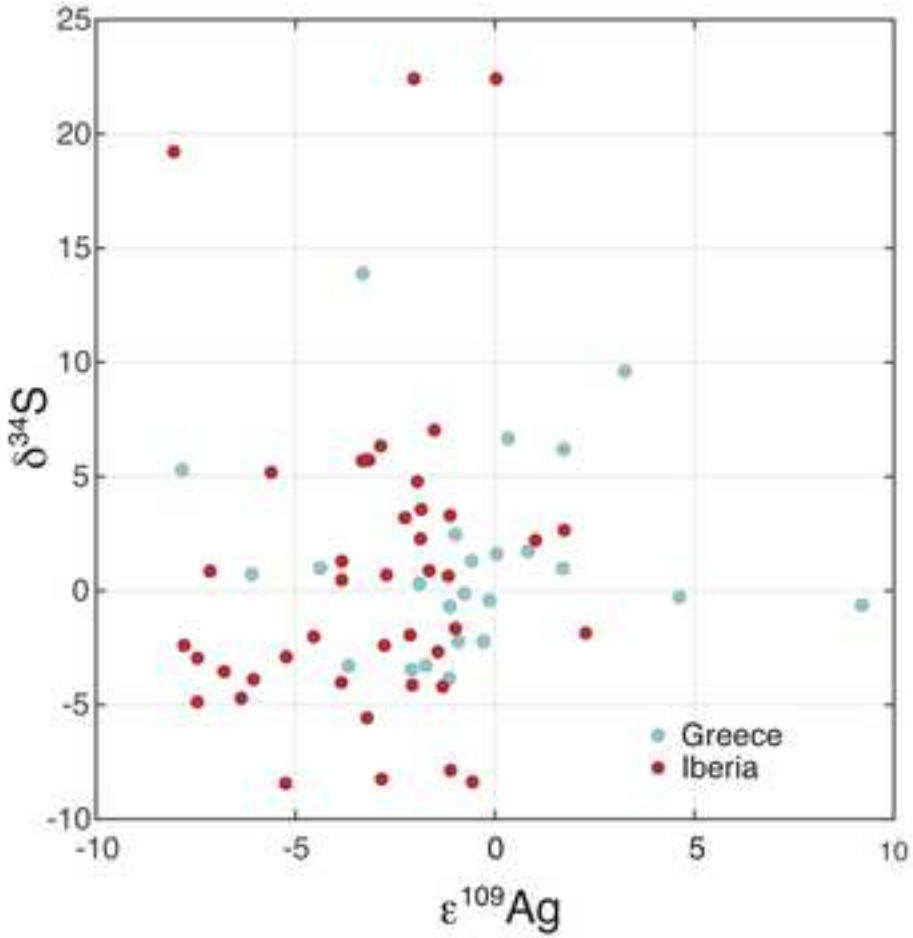

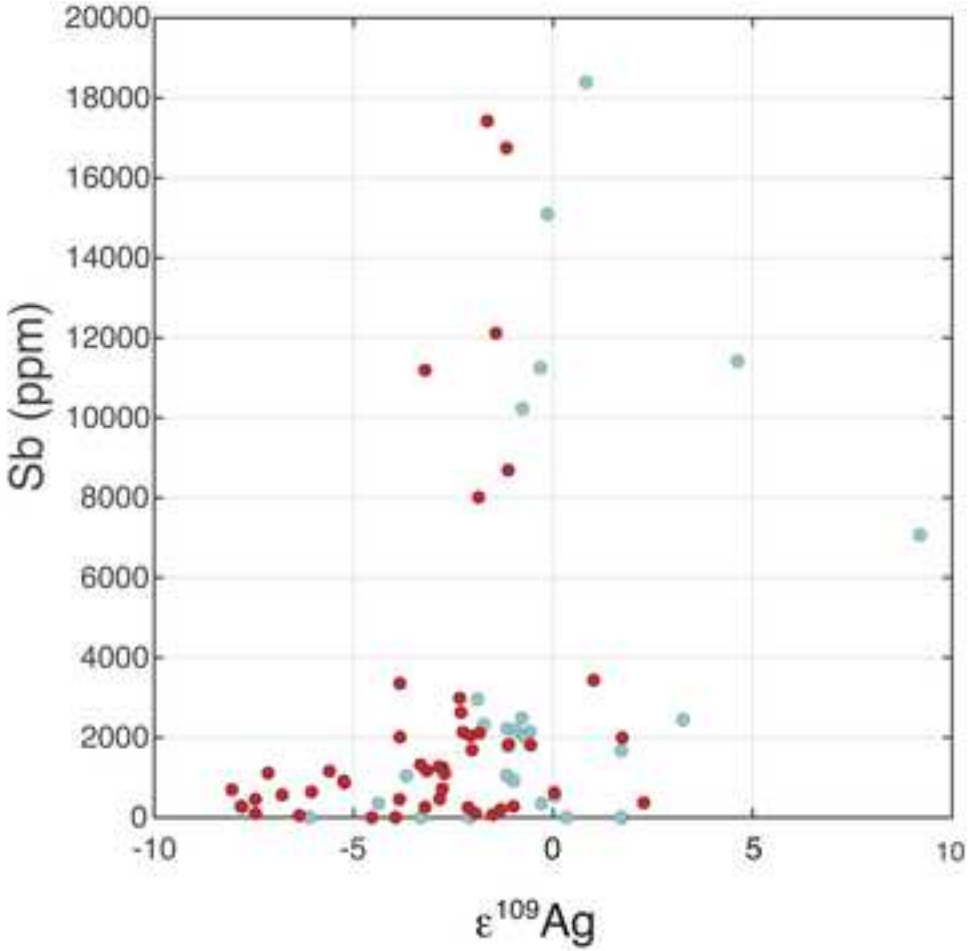

Figure 5

Click here to access/download;Figure;FIG. 05.jpg

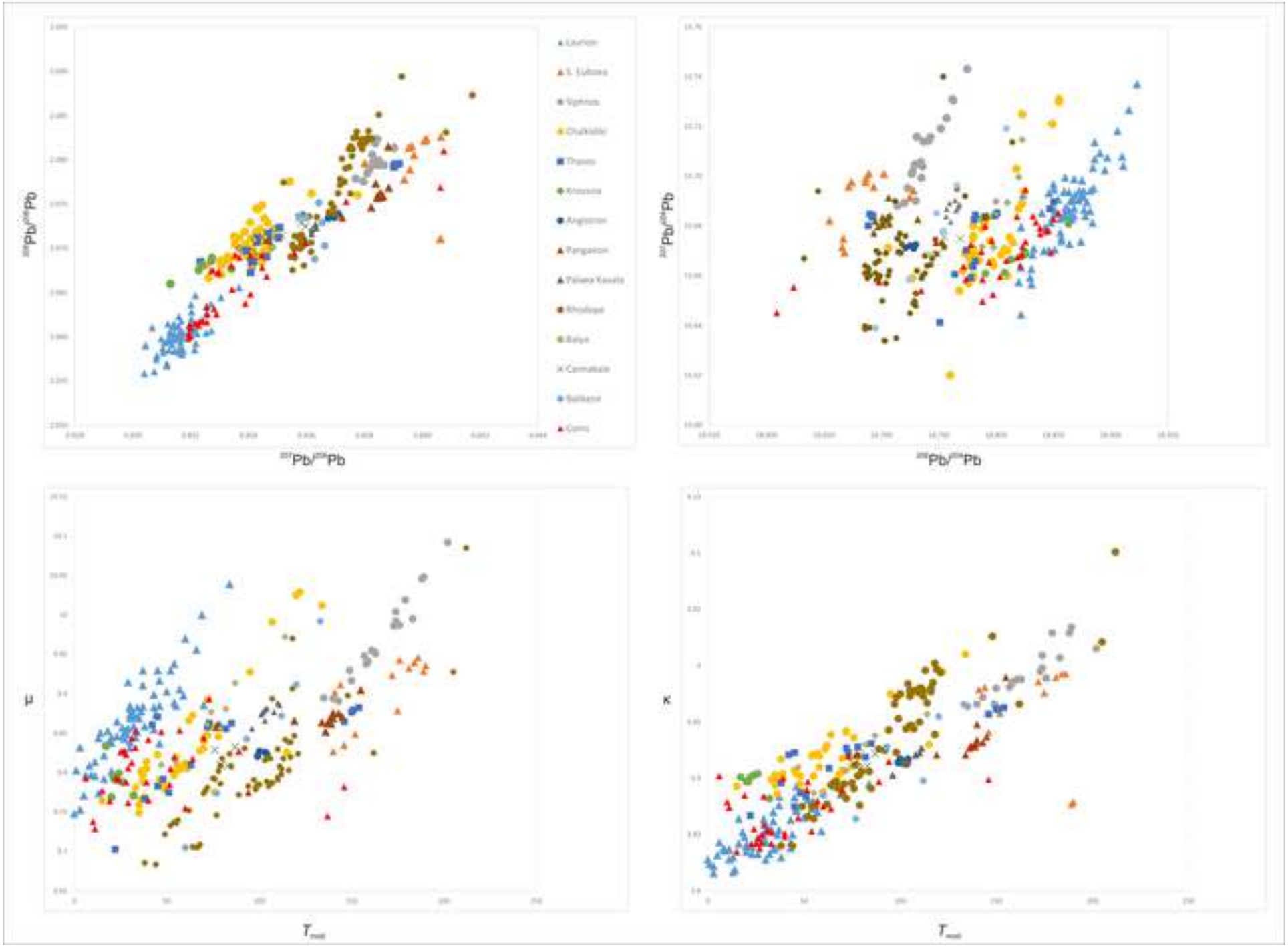

Figure 6

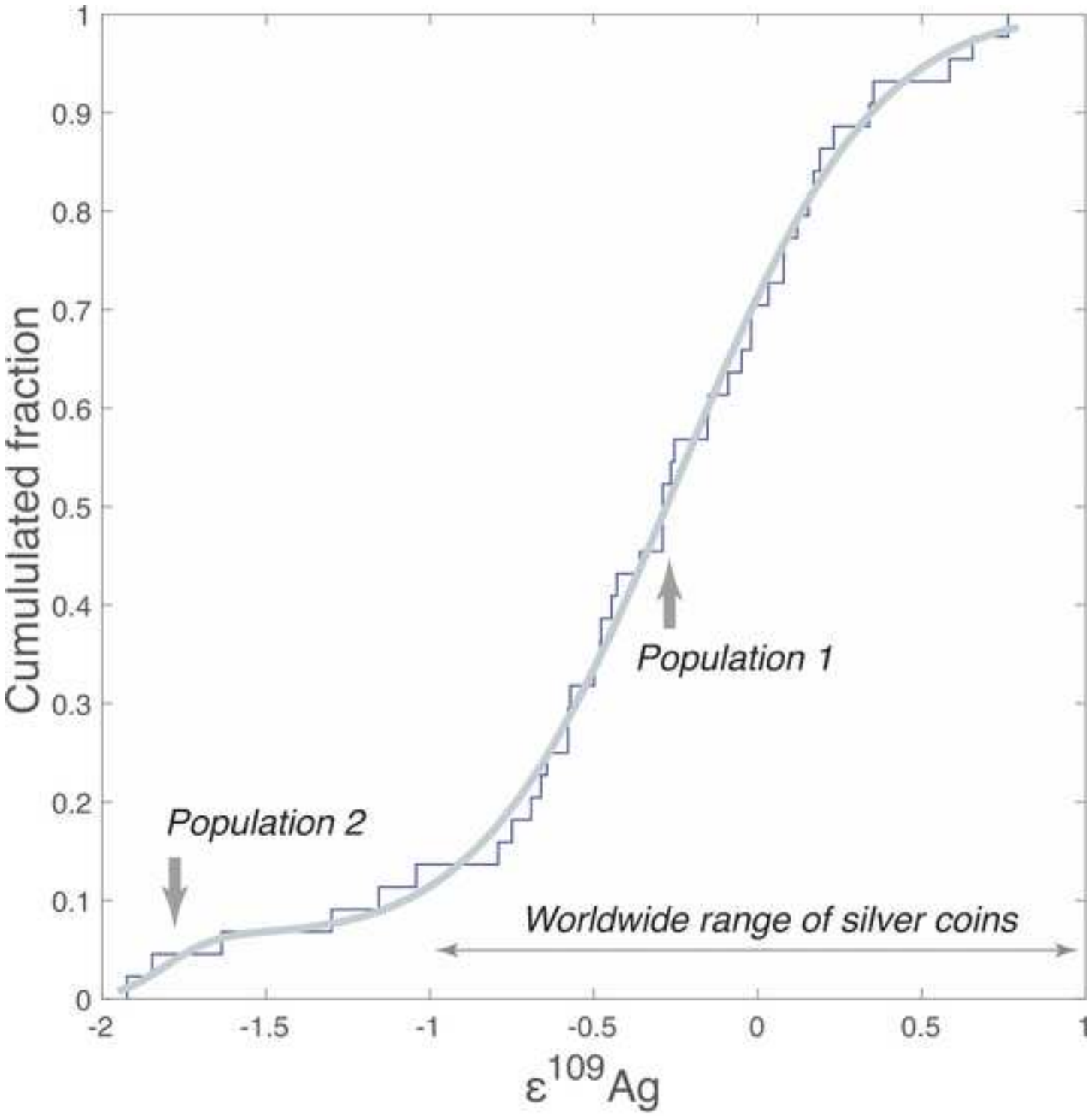

Fig. 07

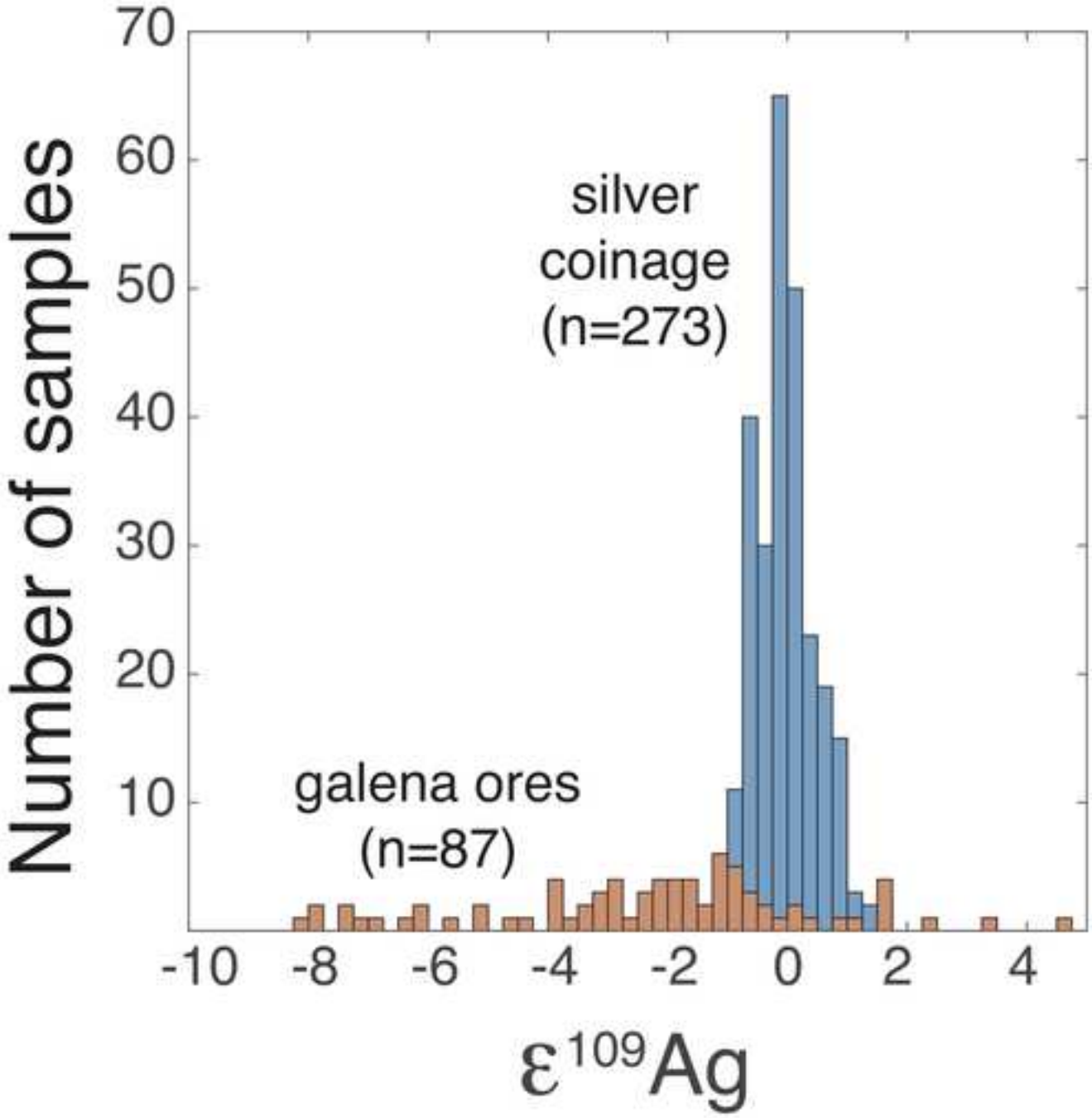

Fig. 08

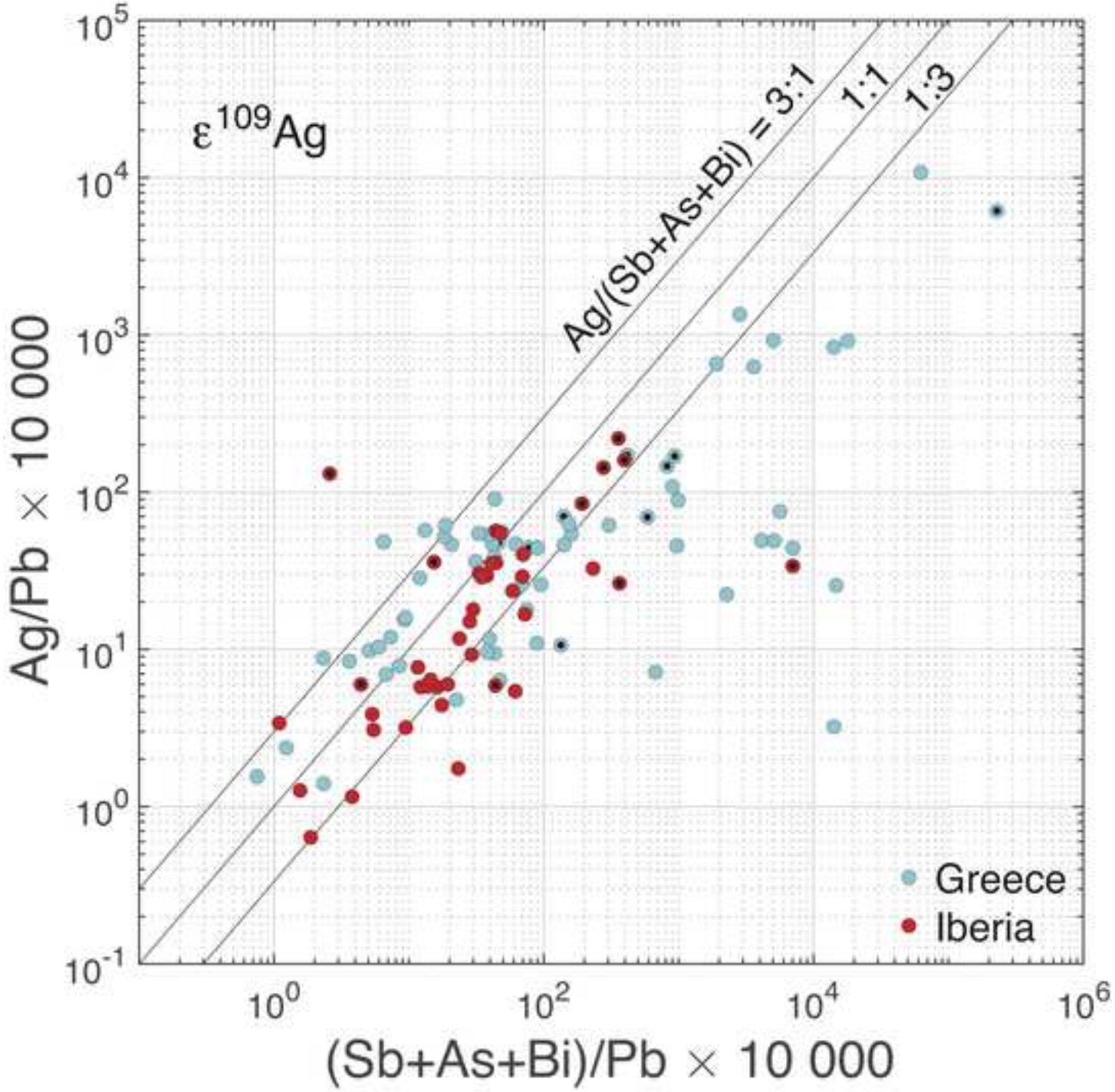

Fig. 09

Click here to access/download;Figure;FIG. 09.jpg